Hindawi
Advances in Civil Engineering
Volume 2023, Article ID 5278404, 13 pages
https://doi.org/10.1155/2023/5278404

Research Article

Study on the Influence of Geometric Parameters and Shape Optimization of Single Tenon Joint in Assembled Subway Station

Bingquan Xiang,[1] Linzhao Cui,[1] Wantao Ding,[2] Wendong Tang,[3] Tengsheng Yue,[1] and Wang Qin[2]

[1]*Anhui Province Key Laboratory of Green Building and Assembly Construction, Anhui Institute of Building Research & Design, Heifei, Anhui 230031, China*
[2]*School of Qilu Transportation, Shandong University, Jinan 250002, China*
[3]*Anhui Construction Engineering Inspection Technology Group Co., Ltd., Heifei, Anhui 230031, China*

Correspondence should be addressed to Wantao Ding; dingwantao@sdu.edu.cn

Received 21 June 2023; Revised 29 August 2023; Accepted 2 September 2023; Published 10 October 2023

Academic Editor: Federico Gusella

The various components of fully prefabricated metro stations are mainly connected using grouted tenon and mortise joints. Therefore, studying the mechanical properties of the joint locations is of significant importance for the overall safety and stability of the station. This paper focuses on the single tenon-long joint as the research object and applies an orthogonal experiment plan to investigate the relationship between the lower bottom length, upper bottom length, and height of the joint and its flexural load carrying capacity. After comparing various loading methods, uniformly distributed loads are chosen as the method for applying axial forces and bending moments. The objective is to determine the dimensions of the tongue and groove that exhibit optimal mechanical properties based on the law of opening displacement and maximum deflection variation with bending moment. The influence of geometrical parameters on the flexural strength of tenon joints is analyzed by means of range analysis in order to find the combination of geometrical parameters with the best mechanical properties. The degree of influence of each geometrical parameter was also ranked. Using these insights, the authors proposed a modified cross-shaped tenon based on the optimal combination of geometrical parameters, which was verified by comparing the M–θ curves of the optimal combination and the optimum working condition. The main conclusions are as follows: (1) the ranking of the geometric parameters of the joint in terms of their influence on the flexural capacity is as follows: height has a greater impact than the bottom length, and the bottom length has a greater impact than the top length. Among these parameters, the influence factor of the height is significantly greater than the other two. (2) The optimum geometry for the tenon and mortise joint is 385 mm for the lower bottom length, 230 mm for the upper bottom length, and 200 mm for the height; the joint's ratio of height to total width should be 25%, the ratio of lower bottom length to total width should be 48%, and the ratio of upper bottom length to total width should be 29%. (3) The load carrying capacity of the cross-shaped tenon is significantly higher than that of the optimal combination and optimum working condition, providing a significant improvement. This research's results will serve as a valuable reference for designing assembly nodes in prefabricated assembly metro stations.

1. Introduction

Prefabricated construction technology is green, fast, and efficient, and has been fully developed and applied in surface construction, but its application in underground construction is still in its infancy [1–3]. Nowadays, the underground building with the most application of prefabricated assembly construction technology and the most practical engineering experience is the metro station, which has been successfully built and applied in many stations of Changchun Metro [4], Qingdao Metro [5], Shenzhen Metro [6], and Jinan Metro [7]. The main structure of an assembled metro station is made up of prefabricated elements that are joined together (as shown in Figure 1(a)), the most common method of joining being the tenon and mortise joint. The mortise and tenon joint is a type of connection in which concave and convex parts are combined on two components. The protruding part is called the tenon, and the indented part is

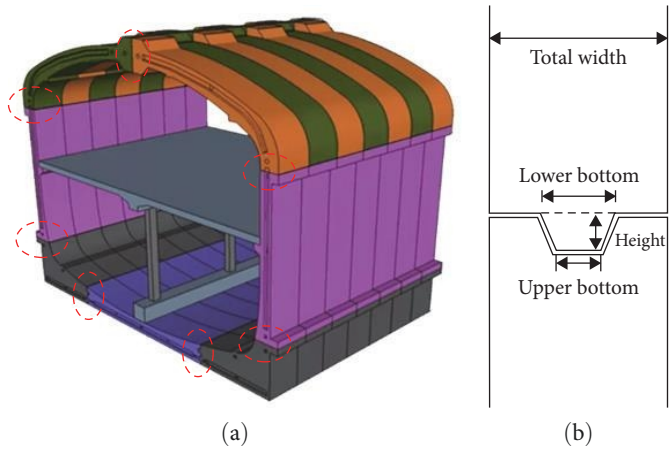

Figure 1: Schematic representation of joint positions and geometric parameters: (a) grouted tenon and mortise joint positions and (b) geometrical parameters of joint.

called the mortise (as shown in Figure 1(b)). It was widely used in wooden architecture [8, 9] and furniture manufacturing. Many scholars have conducted research on the mechanical properties of mortise and tenon structures. Li et al. [10] considered the influence of different levels of damage to the seismic performance of unidirectional straight tenon wood frames. Galassi et al. [11] studied Andalusian timber roof structures in northern Morocco through investigation, analysis, and numerical simulation. Hassan et al. [12] found that the experimental performance of glass fiber reinforced polymer (GFRP) mortise and tenon joints under the tensile loads can be significantly improved. Shanks and Walker [13] studied the pull-out, bending, and shearing behavior of tenons under the different types of wooden nails, and predicted the collapse load of mortise and tenon wooden frame structures using upper-bound plasticity theory. In addition, mortise and tenon joint technology is also commonly used in fields such as prefabricated houses made of reinforced concrete [14], prefabricated underground stations [15], and tunnel linings [16]. The first fully prefabricated metro station in China, Yuanjiadian Station on Line 2 of the Changchun Metro, is connected by the grouted tenon and mortise joints. The tenon and mortise joint is the predominant method of connection in assembled subway stations, and the joint's area is typically the weakest node in the overall station structure [17–19]. At present, the relationship between the geometric characteristics of the joint itself and its load-bearing capacity is not clear, and the design principle of the groove shape also lacks a specific and informative theoretical system. Therefore, it is important to study the mechanical properties of the joint structure for the analysis of the overall force stability of the station.

Some scholars have relied on the actual engineering projects and used model tests and numerical simulations to study the bending stiffness and load-bearing capacity of tenon and mortise joints, achieving a series of results. Yang et al. [20, 21], and Xiuren et al. [22], based on the construction of the Changchun Subway Line 2, conducted model tests on the load-bearing characteristics and failure modes of single-tenon and double-tenon joints of different lengths, proposed a universal calculation formula for bending stiffness, and summarized the variable stiffness characteristics of tenon and mortise joints, laying the foundation for research in this field. Li and Liu [23] studied the factors affecting the bending stiffness of single-tenon joints using numerical simulations, and summarized the variation patterns of bending stiffness under the different conditions such as axial force, tenon and mortise length, width, inclination angle, and grouting. Li et al. [24] conducted model tests to study the evolution of cracks in the concrete structure and the changes in bending stiffness of the double-tenon and mortise joint, and obtained an empirical formula for the bending stiffness of the joint through experimental results and fitting curves. Tao et al. [25] considered the contact relationship between prefabricated components, established a "stratum-solid-contact" calculation model, and studied the influence of different support methods on the internal force, stress, and deformation of the structure. These studies mainly focus on the external factors such as axial force, grouting on the test piece, and there is a lack of systematic and comprehensive research on the influence of geometric parameters of the tenon and mortise joint structure itself. Therefore, in-depth research on the relationship between the geometric parameters of the tenon and mortise joint and its bearing capacity is necessary in order to select the most reasonable tenon and mortise structure form in the different engineering situations.

This paper mainly investigates the influence of the geometric parameters of the single tenon-long joint on its mechanical properties. The lower bottom length, upper bottom length, and height of the tenon and mortise joint were selected as independent variables, and three levels were chosen for each factor in an orthogonal experimental design. Nine sets of three-dimensional finite element numerical models were established and subjected to the same boundary conditions, axial force, and bending moment for the numerical calculation. The maximum deflection at the joint and the opening displacement of the joint were monitored and analyzed, and the best working condition was obtained. Reduced scale model experiments were conducted to verify the reliability of the numerical simulation. The influence of geometrical parameters on the flexural strength of tenon joints is analyzed by means of range analysis in order to find the combination of geometrical parameters with the best mechanical properties. The degree of influence of each geometrical parameter was also

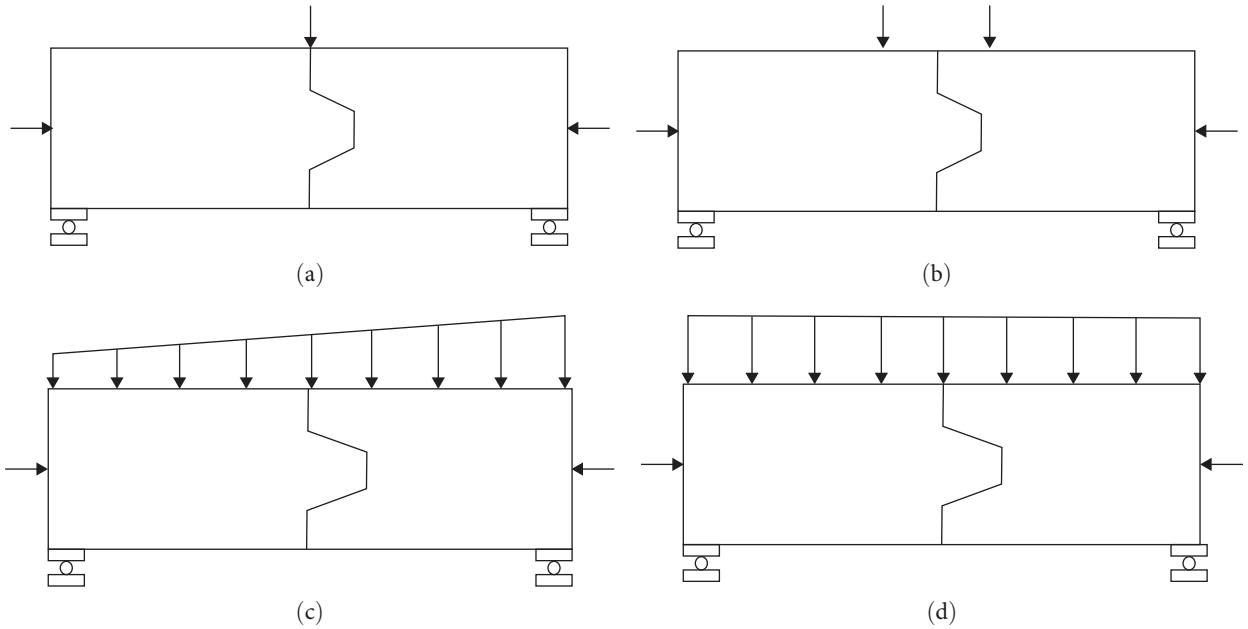

Figure 2: Loading method illustrations: (a) single concentrated load, (b) symmetrical concentrated load, (c) trapezoidal distribution of load, and (d) uniform load.

ranked. Based on the deformation characteristics of the tenon and mortise joint, an optimized and improved cross-shaped tenon and mortise joint was proposed. The M–θ curves of the cross-shaped joint, the optimum working condition, and the optimal combination were compared and analyzed to explore the design of tenon and mortise joints with excellent mechanical properties for modular subway stations.

2. Research Strategy

2.1. Loading Method. In the present study, the loading method of the tenon and mortise joint model was simplified to equivalent concentrated loading, taking into account the practicality and simplicity of the model test. It can be mainly divided into two situations: one is to apply equal concentrated loads at equidistant positions on both sides of the joint (as shown in Figure 2(a)) [26, 27]. This pure-bending loading method reduces the influence of shear force on the test results. The other is to directly apply the concentrated loads at the joint position (as shown in Figure 2(b)) [28, 29]. This loading method has been proven to cause stress concentration at the joint position in practical processes, affecting the stability and accuracy of the test results. These two simplified loading methods have certain advantages, but they do not fully conform to the actual situation. However, in practical situations, the tenon and mortise joints on the station side walls are primarily subjected to earth pressure, which is a trapezoidal surface force that acts over the entire surface (as shown in Figure 2(c)). On the other hand, the tenon and mortise joints on the station top and bottom slabs are subjected to uniformly distributed loads (as shown in Figure 2(d)). In order to select an accurate and convenient loading method, simulations and comparative analyses were carried out for the four loading methods mentioned above. The tenon and mortise joint model is subjected to combined active forces of 750 kN from both the concentrated and distributed loads. Figure 2 shows an illustration of the four different loading methods.

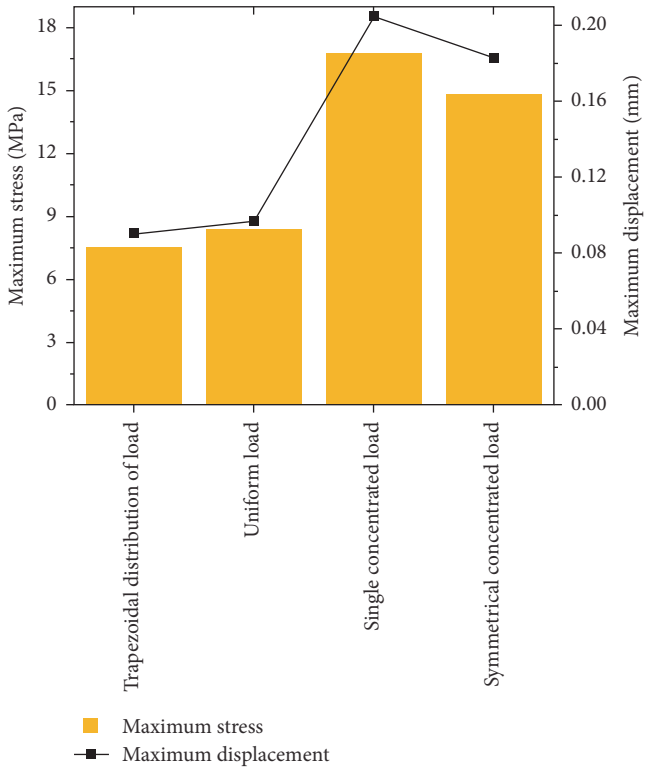

Figure 3: Comparison of calculation results by loading method.

Figure 3 shows the numerical simulation results of maximum stress and maximum displacement under the different loading methods. The maximum stresses and displacements

Table 1: Geometric parameters of the tenon slot for orthogonal test conditions.

Working conditions	Lower bottom length (mm)	Upper bottom length (mm)	Height (mm)
1	335	200	200
2	335	230	280
3	335	265	240
4	360	200	240
5	360	230	200
6	360	265	280
7	385	200	280
8	385	230	240
9	385	265	200

Table 2: Main mechanical properties of concrete.

Density (kg/m^3)	Elastic modulus (N/m^2)	Poisson ratio	Expansion angle (°)	Eccentricity	fb0/fc0
2,400	3.25×10^{10}	0.2	38	0.1	1.16

under distributed loads are only about 50% of those under the concentrated loads; the differences between trapezoidal and uniformly distributed loads, single concentrated loads, and symmetrical concentrated loads are relatively small. Therefore, there is a certain error in using the simplified equivalent concentrated load instead of the actual distributed load as the loading method, and the distributed load is more appropriate to the actual situation. Where the trapezoidal distributed load is influenced by the length of the joint model and the difference in load gradient between the top and bottom ends is small, the effect is almost identical to that of a uniformly distributed load and can be replaced by the equivalent of a uniformly distributed load. Considering the accuracy and simplicity of the simulation, a uniformly distributed load was used as the loading method in this study.

2.2. Design Working Conditions. This paper employs the orthogonal test method to effectively design single tenon and mortise joints with various geometrical parameters. By selecting representative working conditions from the full-scale test in an orthogonal manner, this approach ensures the uniform dispersion and organized comparability of the results. As the number of target types and gradients increases, the number of full-scale tests increases geometrically, making it impossible to analyze the causes using a full-scale test. The orthogonal test method is a good solution to this problem. By replacing the full test with a partial test, the number of tests can be greatly reduced, the test objectives can be achieved efficiently and quickly, and good analytical results can be guaranteed.

In this paper, three geometric factors, namely the length of the lower bottom, the length of the upper bottom and the height of the tenon and mortise, were selected as independent variables, and three levels of each factor were chosen for a three-way, three-level orthogonal test design. The ratio of the lower bottom length to the total width is 43%, the ratio of the upper bottom length to the total width is 28.6%, the ratio of the height to the total width is 28.6% and the ratio of both the upper bottom length and the height to the lower bottom length is 66.7% for commonly used single tenon joint shapes in engineering. On this basis, the orthogonal group was designed for each factor level: 41.8%, 45%, and 48.2% for the ratio of lower base length to total width; 25%, 29%, and 33% for the ratio of upper base length to total width; 25%, 30%, and 35% for the ratio of height to the total width. The joint model has a total length of 2,400 mm, a total width of 800 mm, a total thickness of 1,000 mm, a concrete grade of C40, and a reinforcement type of HRB400. Table 1 shows the geometric design parameters for the tenon slot for each working condition.

3. Numerical Analysis of Tenon and Mortise Joints

3.1. Three-Dimensional Numerical Model. This paper uses the finite element analysis software Abaqus to create a 3D model for numerical calculations. The plastic damage model is used to simulate the intrinsic concrete structure relationship. The model can simulate the hardness degradation mechanism as well as the mechanical properties of concrete with reverse loading stiffness recovery and is suitable for various load analysis of the concrete. The steel bars adopt the elastoplastic hardening model. The steel cage and the concrete adopt built-in constraints, rebar embedded in the concrete. The concrete is modeled using a regular hexahedron solid element, while the steel bars are modeled using a truss element. The contact surface between the tenon and the tenon groove adopts the "surface to surface" contact model, where normal direction utilizes hard contact, leading to direct separation during tension. When compressing, the compressive strength of the contact surface material is considered. The tangential direction adopts penalty friction, with a friction coefficient of 0.2. Tables 2 and 3 list the main mechanical property parameters of reinforced concrete materials. The specific dimensions and the distribution of the working conditions are described in Section 2.2. The model uses a uniform load as the loading method, with

Table 3: Main mechanical properties of HRB400 steel bars.

Density (kg/m^3)	Elastic modulus (N/m^2)	Poisson ratio	Yield strength (N/m^2)
7,800	2×10^{11}	0.3	3.6×10^{8}

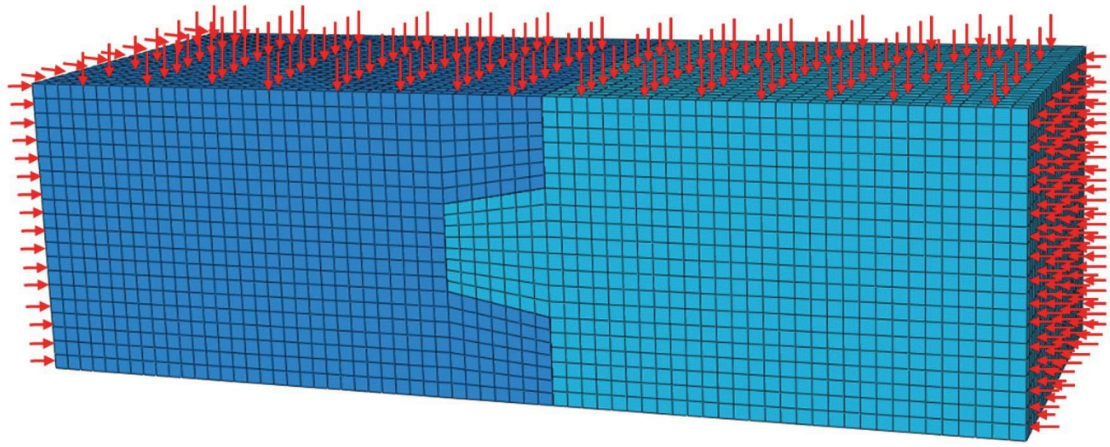

Figure 4: Three-dimensional numerical model loading.

an equivalent uniform load of 1,000 kN for the axial force and increasing bending moments in steps from 100 kN·m. Figure 4 shows how the numerical model is loaded.

3.2. Analysis of the Mechanism for Flexural Capacity of Tenon and Mortise Joints. The opening displacement and maximum deflection were chosen as analysis indicators. The opening displacement refers to the sum of the maximum transverse displacement of the joint model after bending, and the maximum deflection is the maximum vertical displacement at the joint position. The tenon and mortise joint of prefabricated subway stations is different from a continuous structure. It is composed of two independent components, namely the tenon and the mortise, which are fastened together at the joint. Therefore, the mechanism for resisting deformation when bearing bending moment loads is different from that of a continuous structure. When a continuous beam is subjected to bending, the overall deflection is generated based on the assumption of plane section and unidirectional force, and the deflection curve is a continuous function expressed by the equation of the elastic curve. However, when a tenon and mortise joint is subjected to bending, the contact surface is discontinuous, resulting in compression at the upper part of the contact surface and opening at the lower part, causing the two components to gradually separate. After the contact surface between the tenon and mortise components separates, their deflections change differently, and therefore the deflection curve of the two components will break at the contact position, no longer being a continuous curve. Studying the variation law of the maximum deflection and the opening displacement of the contact surface under bending load is of great significance for analyzing the mechanism of the flexural capacity of the tenon and mortise joints.

The variation of the opening displacement at the joint under different working conditions with the change of bending moment is shown in Figure 5. In the initial loading stage, with the increase of bending moment, the opening displacement at the joint in all working conditions is basically 0. The reason for this phenomenon is that the tensile stress on the lower part of the tenon and mortise joint caused by the bending moment is canceled out by the compressive stress generated by the axial force at both ends of the model, so the contact surface hardly separates. However, as the bending moment continues to increase until it reaches 700 kN·m, the opening displacement of the tenon and mortise joints in various working conditions begins to gradually increase, and

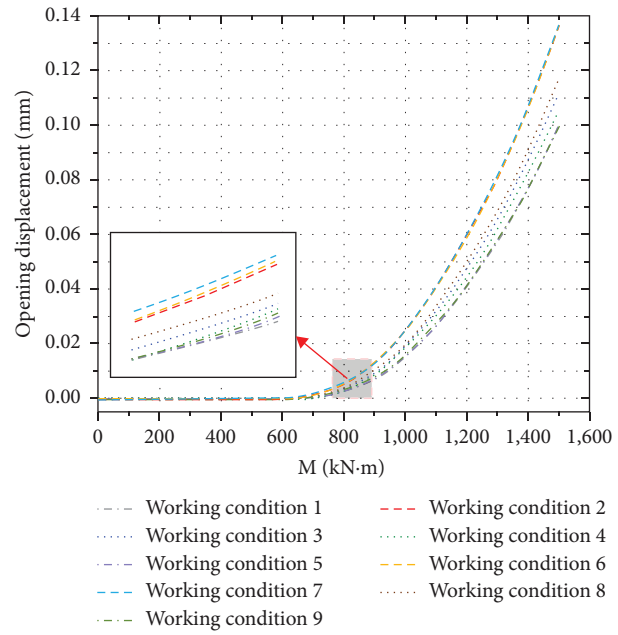

Figure 5: Variation of opening displacement with bending moment. (Numerical analysis).

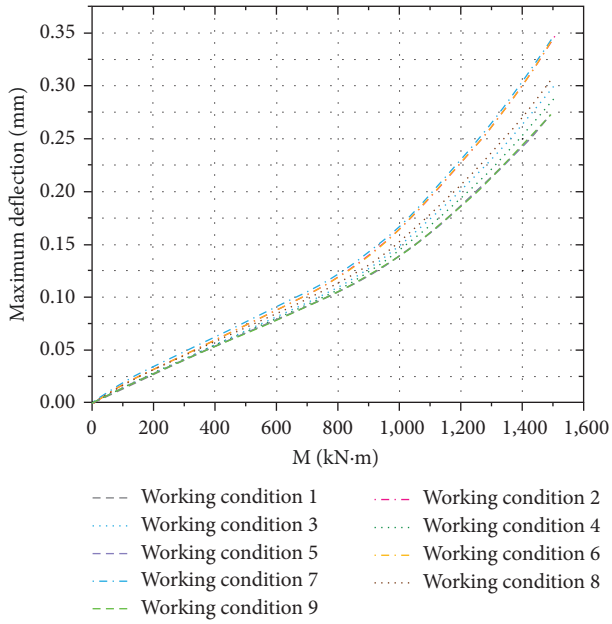

Figure 6: Variation of the maximum deflection with bending moment. (Numerical analysis).

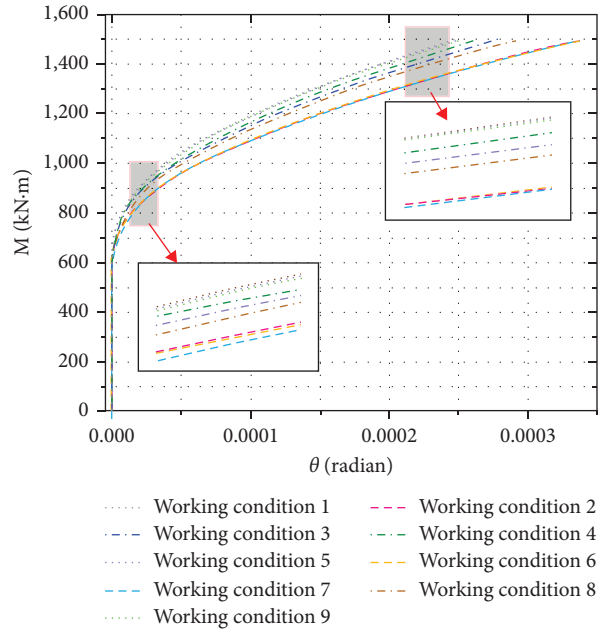

Figure 7: Bending moment–angle variation pattern.

the rate of increase becomes faster and faster. At this time, the influence of the axial force gradually decreases, and the friction force of the embedded joints between the tenon and mortise joints comes into play, and the flexural capacity of the joint structure itself is gradually released. According to the curve development, the nine types of working conditions can be roughly divided into three groups: (1) working conditions 1, 5, and 9; (2) working conditions 3, 4, and 8; (3) working conditions 2, 6, and 7. Comparing with the working condition design in Section 2.1, it is found that the first group corresponds to all working conditions with a tenon and mortise height of 200 mm, the second group corresponds to all working conditions with a tenon and mortise height of 240 mm, and the third group corresponds to all working conditions with a tenon and mortise height of 280 mm. This indicates that the tenon and mortise height is the most obvious geometric factor affecting the opening displacement.

Under the same bending moment, the opening displacement in the first group of working conditions is the smallest, and the opening displacement in the third group is the largest, indicating that the flexural capacity is strongest when the tenon and mortise height is 200 mm, and weakest when the height is 280 mm. Among them, the bearing capacity of working condition 9 is the strongest, making it the best working condition. This phenomenon shows that the tenon and mortise height has the greatest impact on the flexural capacity of the joint, and as the height increases, the opening displacement and maximum deflection gradually increase. Therefore, a larger tenon and mortise height is not better.

From Figure 6, it can be observed that the maximum deflection at the joint increases approximately linearly with the increase of bending moment for each working condition. Before the bending moment reaches 800 kN·m, the embedded frictional force between the mortise and tenon joints directly affects the stiffness of the joint, which results in a slower linear growth rate of the curve. However, after the bending moment increases to 800 kN·m, the slope of the curve significantly increases, indicating that the bearing limit of the mortise and tenon joint has been reached. The stiffness of the joint gradually decreases, leading to a weakening resistance to the bending moment. As the bending moment increases, the deflection of the joint increases rapidly.

The joint bending stiffness k refers to the bending moment required to produce a unit rotation angle of the joint and is a critical indicator of the joint's bending deformation resistance. The joint turning angle θ can be calculated using the tension amount at the joint [12]. Previous studies have demonstrated that tenon and mortise joints exhibit varying stiffness properties [12, 20]. The slope of the M–θ curve of the joint represents its bending stiffness k, which can directly reflect the remodeling pattern of the joint's bending stiffness.

Figure 7 reflects the bending moment-rotation angle change relationship for all working conditions. It can be seen that in the initial loading stage, as the bending moment increases, the joint angle is almost zero, indicating that at this time the joint does not produce a corner due to the action of the axial force, and the bending stiffness is great. As the bending moment continues to increase to 700 kN·m, deflection gradually occurs and the required bending moment to produce the same deflection also decreases, indicating that continued loading will gradually reduce the stiffness of the joint, and the bearing capacity of the tenon and mortise joint gradually weakens and begins to fail. Additionally, the third group of curves first shows an inflection point, with the largest deflection at the same bending moment, indicating that as the bending moment gradually increases, the third group first starts to produce deflection, and its ability to resist bending deformation is the weakest; the first group shows an inflection point last with the smallest deflection at the same

Figure 8: The entire process of the model test.

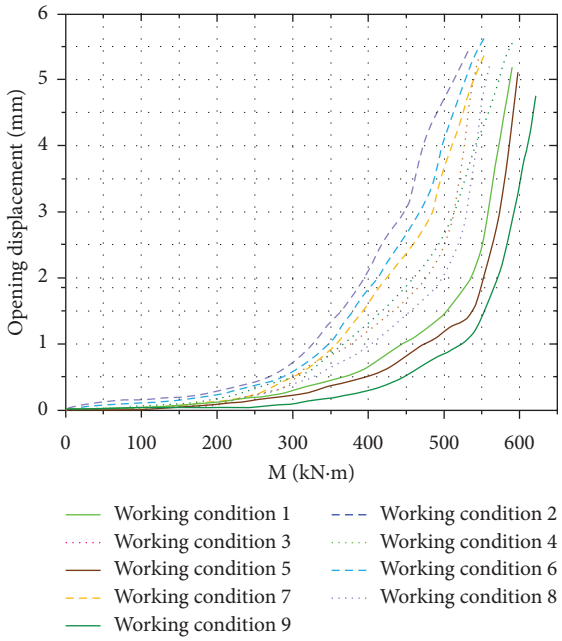

Figure 9: Variation of opening displacement with bending moment. (Model test).

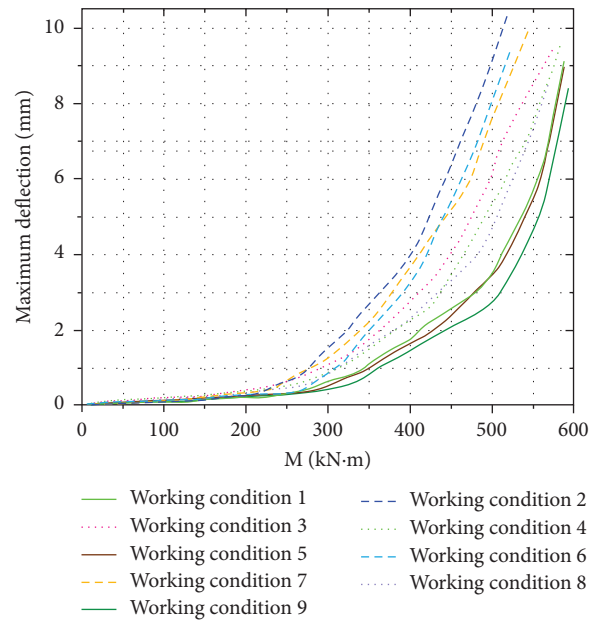

Figure 10: Variation of the maximum deflection with bending moment. (Model test).

bending moment, indicating that the first group produces deflection last, and its ability to resist bending deformation is the strongest. Furthermore, within the first group, operating condition 9 performs the best.

3.3. Comparison with Reduced-Scale Model Test Result. To verify the accuracy of the numerical simulation results, reduced-scale model tests were conducted to study the flexural capacity of the tenon and mortise joint under the various working conditions (Figure 8). The test results are shown in Figures 9 and 10, demonstrating the opening amount and maximum deflection with bending moment for tenon and mortise joint with different geometric parameters.

(1) It can be observed that the curves of the experimental results have the same development trend as the simulation results: the curves of all working conditions grow slowly at the initial stage, and then begin to develop as the moment increases. With the increase in moment, the opening amount and maximum deflection at the joint position gradually increase, and the growth rate increases.

(2) According to the speed of growth, the curves of all working conditions can be divided into three groups: (1) working conditions 1, 5, and 9; (2) working conditions 3, 4, and 8; (3) working conditions 2, 6, and 7. This corresponds exactly to the three different tenon and mortise heights, which proves that the tenon and mortise height has the greatest influence on the opening amount and maximum deflection of the tenon and mortise joint, and the influence is much greater than that of the bottom and upper bottom

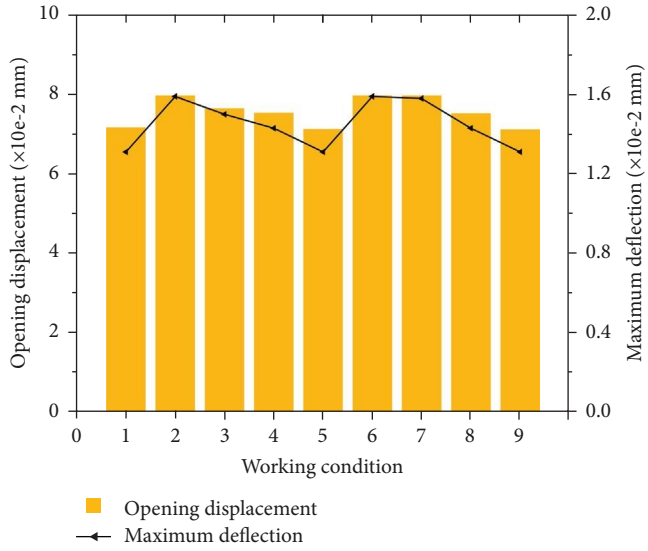

Figure 11: Summary of calculation results.

Table 4: Result of range analysis for opening displacement.

	Lower bottom length (mm)	Upper bottom length (mm)	Height (mm)
$K1$ ($\times 10^{-3}$)	227.91	226.87	214.23
$K2$ ($\times 10^{-3}$)	226.44	226.26	227.30
$K3$ ($\times 10^{-3}$)	226.26	227.48	239.07
$k1$ ($\times 10^{-3}$)	75.97	75.62	71.41
$k2$ ($\times 10^{-3}$)	75.48	75.42	75.77
$k3$ ($\times 10^{-3}$)	75.42	75.83	79.69
R ($\times 10^{-3}$)	0.55	0.41	8.28
The optimal combination	3	2	1

lengths of the tenon and mortise, which is consistent with the conclusion of the numerical simulation results.

(3) Among the three curves of the first group with a tenon and mortise height of 200 mm, the opening amount and maximum deflection are the smallest under the same moment; among the third group with a tenon and mortise height of 280 mm, the opening amount and maximum deflection are the largest, indicating that the joint has the strongest flexural capacity when the tenon and mortise height is 200 mm, among which working condition 9 is the strongest of all working conditions. When the tenon and mortise height is 280 mm, the flexural capacity of the joint is the weakest, which is consistent with the simulation results.

(4) The values of the opening amount and maximum deflection in the experimental results are significantly different from the numerical simulation results. The analysis of the reasons mainly includes three points: First, in the loading process, there are unavoidable gaps between the mortise and tenon joint model and the actuator. These gaps gradually close during the loading process, which can cause errors in displacement. Second, numerical simulation cannot simulate the fracture phenomenon of concrete, while in the experiment, cracks will occur in the joint when it reaches the ultimate load, and these cracks will quickly expand with the increase of bending moment, resulting in a large displacement which leads to a much larger displacement value in the model test than in the numerical simulation. Third, the experimental group used a scaled model test while the control group used a full-scale simulation, which has a certain influence on the results due to the size effect.

3.4. Orthogonal Experimental Range Analysis. The calculation results for axial force of 1,000 kN and bending moment of 1,000 kN·m were selected for analysis. Figure 11 shows the calculation results for the opening displacement and maximum deflection of each experimental group.

Opening distance and maximum deflection of tenon and mortise joints under different working conditions were processed by extremum difference analysis. The range analysis table for opening distance is shown in Table 4, and the range analysis table for maximum deflection is shown in Table 5. $K1$, $K2$, and $K3$ represent the sum of the judgment indicators for a certain factor at three levels, and $k1$, $k2$, and $k3$

Table 5: Result of range analysis for the maximum deflection.

	Lower bottom length (mm)	Upper bottom length (mm)	Height (mm)
$K1$ ($\times 10^{-3}$)	439.86	431.55	392.05
$K2$ ($\times 10^{-3}$)	432.82	432.68	436.37
$K3$ ($\times 10^{-3}$)	431.49	439.94	475.75
$k1$ ($\times 10^{-3}$)	146.64	144.56	130.68
$k2$ ($\times 10^{-3}$)	144.27	143.86	145.46
$k3$ ($\times 10^{-3}$)	143.83	146.65	158.58
R ($\times 10^{-3}$)	2.81	2.79	27.90
The optimal combination	3	2	1

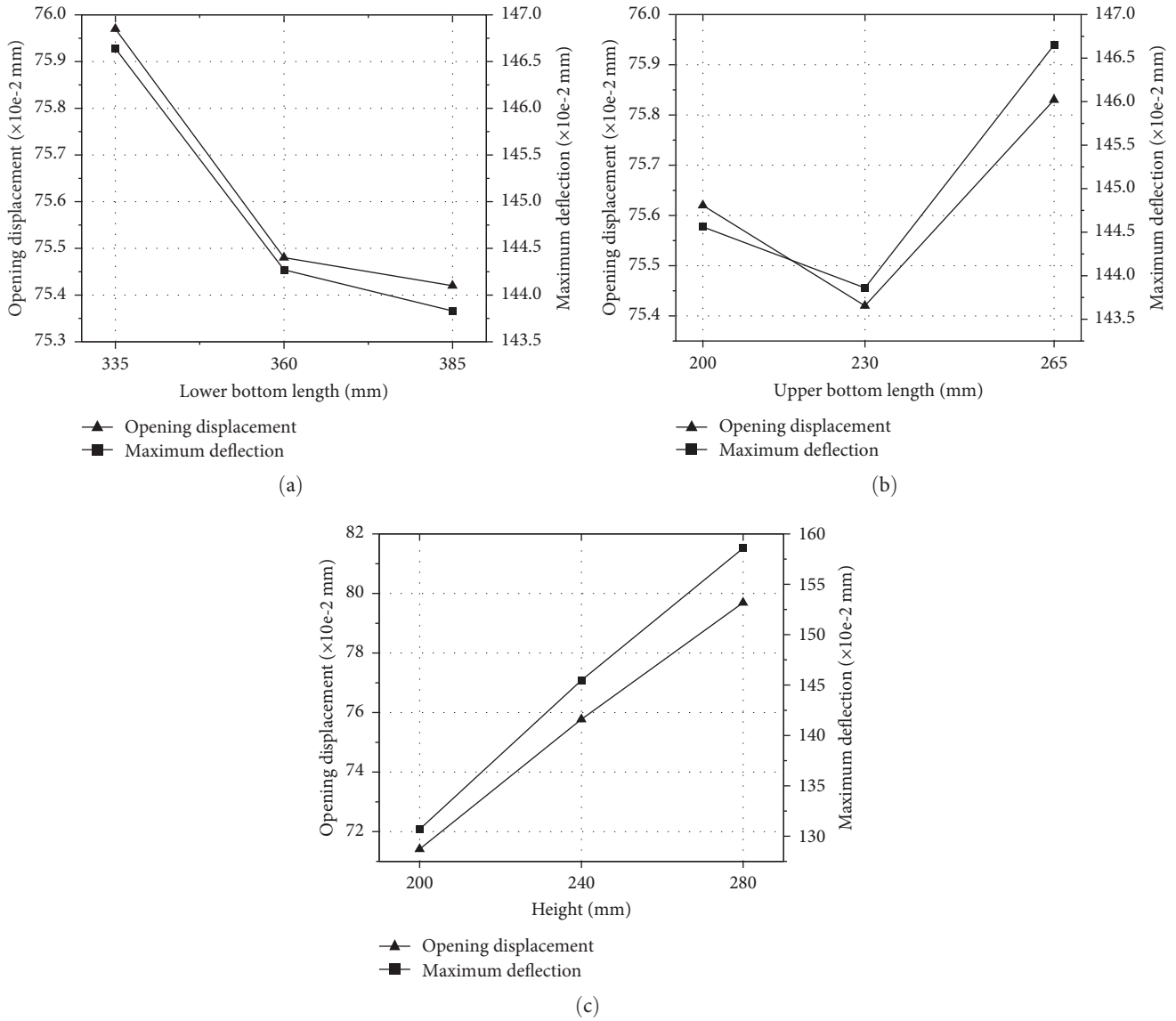

Figure 12: Average of tension and maximum deflection at each geometric level: (a) lower bottom length, (b) upper bottom length, and (c) height.

represent the average value of this factor at the three levels. R represents the range.

The smaller the opening displacement and the maximum deflection of the joint, the stronger the resistance of the tenon and mortise joint to deformation and the better its bending load-bearing capacity. The average values of the opening distance and maximum deflection for each factor at three levels are shown in Figure 12. It can be seen that they have

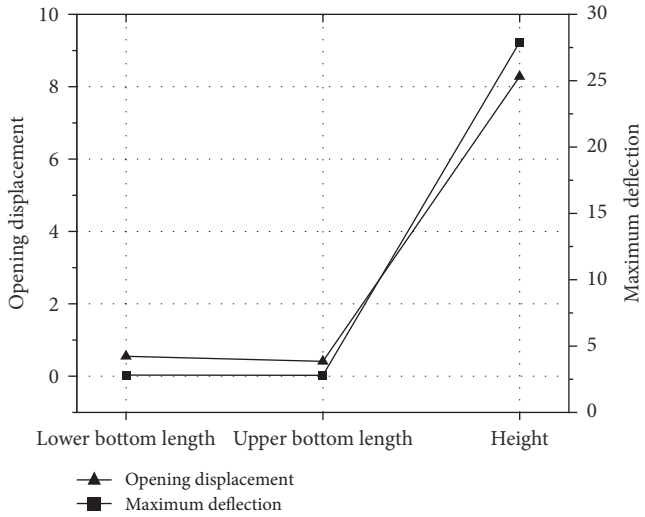

Figure 13: Comparison of geometric parameter ranges.

the same changing pattern: for the lower bottom length, the level with the smallest average value is Level 3; for the upper bottom length, Level 2 has the smallest average opening distance; and for the height, Level 1 has the smallest average opening distance. This indicates that the optimal combination of geometric dimensions for tenon and mortise joint is 3–2–1, i.e., the lower bottom length of 385 mm, the upper bottom length of 230 mm, a height of 200 mm. With the increase of lower bottom length, the opening distance and maximum deflection at the joint position gradually decrease, indicating that properly increasing the bottom length can improve the bearing capacity of the tenon and mortise joint. With the increase of upper bottom length, the opening distance and maximum deflection first decrease and then increase, indicating that increasing or decreasing the upper bottom length on the basis of the second level will weaken the bearing capacity of the tenon and mortise joint, and keeping the upper bottom length/total width at around 29% is most appropriate. With the increase of height, the opening distance and maximum deflection gradually increase, indicating that a larger height for a single tenon joint does not necessarily mean better performance, and properly reducing the height based on existing commonly used single tenon joints can enhance the bearing capacity of the tenon and mortise joint.

The distributions of the polarities corresponding to each of the tenon geometric parameters are shown in Figure 13. The independent variables are the three geometric factors—lower bottom length, upper bottom length, and height. The dependent variables are the opening displacement and maximum deflection of the joint model. The larger value of the extreme deviation represents the larger fluctuation of the dependent variable when the independent variable changes, i.e., the larger degree of influence of the independent variable on the dependent variable. Observing Figure 13, it can be found that when the dependent variable is the opening displacement, the height corresponds to the largest extreme deviation, followed by the lower bottom length, and the upper bottom length corresponds to the smallest extreme deviation, in which the extreme deviation value of the height is much larger than the other two. And the same conclusion is also found when the maximum deflection is the dependent variable. This indicates that the influence of the geometrical parameters of the joint on the flexural load carrying performance is stronger in the order of height than lower bottom length and upper bottom length, where the influence factor of height is much larger than the other two.

4. Optimized Cross-Shaped Tenon and Mortise Joint

4.1. Numerical Simulation of the Cross-Shaped Joint. During the process of conducting model tests, it was found that the contact surface of a single tenon and mortise joint was prone to open up when subjected to bending moment, and this could even cause the test piece to slip. The analysis revealed that the cross-sectional shape of the single tenon and mortise joint was trapezoidal, which made it susceptible to relative sliding when subjected to bending moment, as shown in Figure 14. To address this problem, an optimized cross-shaped tenon and mortise joint was proposed based on the optimal combination of single tenon and mortise joints: a secondary tenon perpendicular to the primary tenon was added at the midpoint of the primary tenon, with the cross-sectional shape of the secondary tenon being rectangular, in order to enhance the bending moment resistance cross-section of the tenon and mortise joint and weaken the relative sliding effect of the contact surface. The size of the primary tenon in the cross-shaped tenon and mortise joint was selected as the best horizontal combination obtained in Section 3.4: a bottom width of 385 mm, a top width of 230 mm, and a height of 200 mm. The height of the secondary tenon was identical to that of the primary tenon, at 200 mm, with a width of 200 mm and a length of 600 mm. Figure 15 shows the structure of the cross-shaped tenon and mortise joint. Under the same conditions of material properties, meshing, and loading position, numerical simulations were conducted to simultaneously load the axial force and bending moment on the optimal combination of the cross-shaped tenon and mortise joint and the single tenon and mortise joint.

4.2. Comparative Analysis of Flexural Stiffness. Compare and analyze the M–θ curve of working condition 9, the optimal geometric parameters and the cross-shaped mortise are shown in Figure 16. It can be seen that the three curves have similar development trends overall, undergoing two periods of linear and nonlinear stages. In the linear stage, as the bending moment increases, the angle deformation is very small and almost zero, and the bending stiffness is relatively large, which is the main bearing stage of the joint. In the nonlinear stage, as the bending moment increases, the rate of angle deformation gradually increases and the rate of reduction in bending stiffness accelerates, indicating that the joint undergoes a softening phenomenon. In the initial period of the nonlinear stage, the slope is still relatively large, indicating that the joint has not reached its bearing limit and still has certain bending stiffness and relatively stable bearing

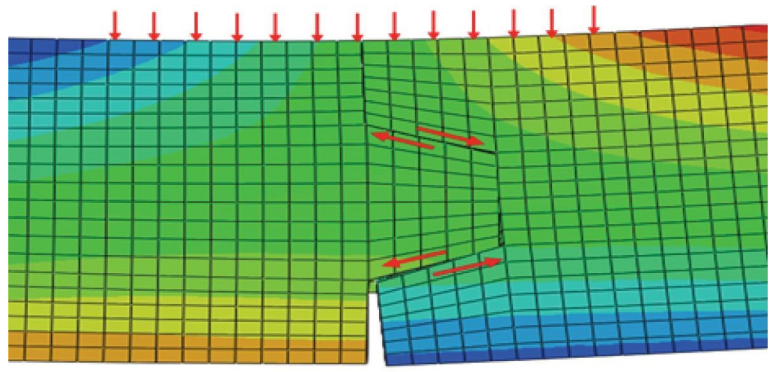

Figure 14: Relative sliding tendency of contact surfaces.

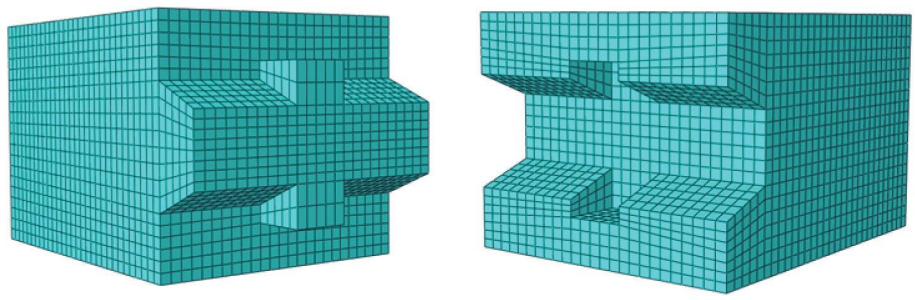

(a) (b)

Figure 15: Illustration of the cross-shaped tenon and mortise joint: (a) tenon and (b) mortise.

capacity. However, when the curve tends to be flat, the bending stiffness is extremely small, indicating that the joint has reached its bearing limit and may collapse at any time. Therefore, in the use of tenon and mortise joints, it is necessary to ensure that the working conditions are in the linear stage as much as possible, during which the joint has large bending stiffness, stable bearing capacity, and higher safety.

However, there are also significant differences among the three curves: the overall trend of the optimal combination and working condition 9 is closer, both gradually generating angle at around 700 kN·m, while the cross-shaped tenon and mortise joint does not generate angle until 800 kN·m. The time for the M–θ curve of the cross-shaped tenon and mortise joint to exhibit inflection points is later than that of the optimal combination and working condition 9. Moreover, after the angle appears, the slope of the curve of the cross-shaped tenon and mortise joint is greater than that of the other two curves, and the slope of the optimal combination curve is slightly greater than that of the working condition 9. Under the same bending moment, the angle generated by the cross-shaped tenon and mortise joint is much smaller than that of the other two curves, with the optimal combination being slightly smaller than the working condition 9. These results indicate that the bending bearing capacity of the cross-shaped tenon and mortise joint is significantly better than that of the optimal combination and working condition 9, while the bearing capacity of the optimal combination is slightly better than that of working condition 9. Therefore, the cross-shaped tenon and mortise joint structure has a good optimization effect and is of reference value for improving the bearing capacity and stability of the tenon and mortise joints.

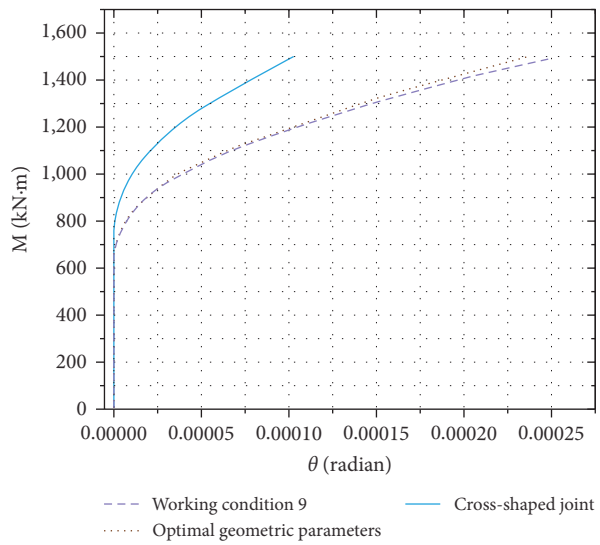

Figure 16: Comparison of M–θ curves.

5. Conclusions

Numerical simulations and model experiments were conducted to study the combined effect of axial force and

bending moment on single long tenon and mortise joints with different geometric parameters. Analysis was conducted on variables such as deflection and maximum bending stiffness to reveal the bending load capacity and its mechanism of tenon and mortise joints with different geometric parameters. Orthogonal analysis was conducted to determine the degree of influence of the tenon and mortise joint's geometric parameters and the optimal combination of parameters. Based on the optimal combination, an improved cross-shaped tenon and mortise joint was proposed and validated, leading to the following conclusions:

(1) The bending load capacity was the best under condition 9 among all conditions. The optimal combination of geometric parameters for tenon and mortise joints was found to be the lower bottom length of 385 mm, upper bottom length of 230 mm, and height of 200 mm, which did not belong to any of the 9 conditions. By comparing the M–θ curves, it was found that the optimal combination had a stronger bending load capacity than condition 9, validating the correctness of the range analysis.

(2) The ranking of the geometric parameters of the joint in terms of their influence on the bending load-carrying capacity is as follows: height has a greater impact than the bottom length, and the bottom length has a greater impact than the top length. Among these parameters, the influence factor of the height is significantly greater than the other two. In addition, a larger height did not necessarily result in better performance. Instead, an appropriate reduction in height while maintaining a ratio of height to total width of around 25% based on commonly used joints in engineering was found to be optimal.

(3) An optimized cross-shaped tenon and mortise joint was proposed based on the optimal combination, and its load-bearing capacity was found to be significantly better than the original single long tenon and mortise joint, indicating a clear improvement in the load-bearing capacity of tenon and mortise joints.

Data Availability

The data used to support the findings of this study are available from the corresponding author upon request.

Conflicts of Interest

The authors declare that there is no conflict of interest regarding the publication of this paper.

Authors' Contributions

Bingquan Xiang contributed in the methodology and writing original draft. Wantao Ding and Wendong Tang contributed in the review and editing. Wendong Tang and Wang Qin contributed in the formal analysis. Linzhao Cui contributed in the conceptualization. Tengsheng Yue contributed in the investigation and validation. Wendong Tang contributed in the resources. Wang Qin and Wantao Ding contributed in the data curation and validation.

Acknowledgments

This study was supported by Open Research Fund of Anhui Province Key Laboratory of Green Building and Assembly Construction, Anhui Institute of Building Research & Design, Grant No. 2022-JKYL-005. The authors thank to the Geotechnical and Structural Engineering Research Center, Shandong University for providing the test data.

References

[1] J. G. Guo and Y. W. Wang, "Study on overall seismic performance of partially prefabricated assembled metro underground station structure," *Earthquake Engineering and Engineering Vibration*, vol. 41, no. 5, pp. 215–224, 2021.

[2] J. Fang, *Study on Mechanical Behavior of Partially Prefabricated Assembled Metro Station*, Southwest Jiaotong University, 2021.

[3] H. F. Su, W. N. Liu, and F. C. Liu, "Preliminary ideas of the metro station constructed by shield tunneling method combined with prefab-ricated method," *Applied Mechanics and Materials*, vol. 580–583, pp. 1013–1018, 2014.

[4] P. J. Jia and W. Zhao, "Study on ground settlement and structural deformation for large span subway station using a new presupporting system," *Royal Society Open Science*, vol. 6, Article ID 181035, 2019.

[5] D. Wang, *Mechanical Properties of Support, Beam and Continuous Wall Joints in Assembled Metro Stations*, South China University of Technology, 2019.

[6] X. Y. Wang, "Key technologies of intelligent design for new type of assembled metro station," *Railway Standard Design*, vol. 66, no. 2, pp. 117–123, 2022.

[7] X. R. Yang, "Current status and prospects of construction technology of prefabricated assembled metro stations in China," *Tunnel Construction (Chinese and English)*, vol. 41, no. 11, pp. 1849–1870, 2021.

[8] R. Hassan, A. Ibrahim, and Z. Ahmad, "Structural behaviour of mortise and tenon joints," in *Timber Connections*, Springer Briefs in Applied Sciences and Technology, Springer, Singapore, 2023.

[9] Y. Z. Erdil, A. Kasal, and C. A. Eckelman, "Bending moment capacity of rectangular mortise and tenon furniture joints," *Forest Products Journal*, vol. 55, pp. 209–213, 2005.

[10] S. Li, Z. Zhou, H. Luo, G. Milani, and D. Abruzzese, "Behavior of traditional Chinese mortise–tenon joints: experimental and numerical insight for coupled vertical and reversed cyclic horizontal loads," *Journal of Building Engineering*, vol. 30, Article ID 101257, 2020.

[11] S. Galassi, L. Dipasquale, N. Ruggieri, and G. Tempesta, "Andalusian timber roof structure in Chefchaouen, Northern Morocco: construction technique and structural behavior," *ASCE's Journal of Architectural Engineering*, vol. 24, no. 3, 2018.

[12] R. Hassan, A. Ibrahim, and Z. Ahmad, "Experimental performance of mortice and tenon joint strengthened with glass fibre reinforced polymer under tensile load," in *2012 IEEE Symposium on Business, Engineering and Industrial Applications*, pp. 856–860, Bandung, Indonesia, 2012.

[13] P. Shanks J. D.& Walker, "Experimental performance of mortise and tenon connections in green oak," *The Structural Engineer*, vol. 83, pp. 40–45, 2005.
[14] R. H. Sangree and B. W. Schafer, "Experimental and numerical analysis of a halved and tabled traditional timber scarf joint," *Construction and Building Materials*, vol. 23, no. 2, pp. 615–624, 2009.
[15] S.-J. Pang, J.-K. Oh, J.-S. Park, C.-Y. Park, and J.-J. Lee, "Moment-carrying capacity of dovetailed mortise and tenon joints with or without beam shoulder," *Journal of Structural Engineering*, vol. 137, no. 7, pp. 785–789, 2011.
[16] L. Rozsa, "Precast concrete segment lining of the Budapest metro," *Tunnels & Tunnelling International*, vol. 11, no. 10, 1979.
[17] M. Zhu, X. H. Sun, and X. S. Chen, "Thinking on green, efficient and intelligent construction of metro underground stations," *Tunnel Construction (Chinese and English)*, vol. 41, no. 12, pp. 2037–2047, 2021.
[18] J. H. Chen, "Research on construction technology of prefabricated assembled metro station," *Railway Construction Technology*, vol. 11, pp. 62–65, 2015.
[19] T. Qiu, D. Su, X. Chen et al., "A novel interfaces contact model for analyzing assembled joints of prefabricated underground structures," *Tunneling and Underground Space Technology*, vol. 133, Article ID 104936, 2023.
[20] X. R. Yang, F. Lin, and M. Q. Huang, "Experimental study on bending bearing capacity of grouted mortise and tenon long joints for prefabricated assembled structures of metro station," *Journal of Civil Engineering*, vol. 53, no. 4, pp. 111–118 128, 2020.
[21] X. R. Yang, F. Lin, and M. Q. Huang, "Experimental study on bending stiffness of grouted mortise and tenon joints for prefabricated assembled structures of metro station," *Journal of Civil Engineering*, vol. 53, no. 3, pp. 38–43, 2020.
[22] Y. Xiuren, H. Meiqun, P. Zhiyong, and L. Fang, "Calculation of dynamic assembly and tensioning loads at multiple points of prefabricated structure," *Tunneling and Underground Space Technology*, vol. 126, Article ID 104564, 2022.
[23] X. W. Li and Q. Liu, "Analysis of influencing factors of bending stiffness of mortise and groove joints of prefabricated assembled metro station," *Railway Standard Design*, vol. 60, no. 8, pp. 113–117, 2016.
[24] Z. P. Li, H. F. Su, and S. Q. Lv, "Experimental study on bending mechanical properties of double mortise and groove joints of assembled metro station structures," *Journal of Civil Engineering*, vol. 50, no. S2, pp. 28–32, 2017.
[25] L. J. Tao, Z. Y. Li, X. R. Yang, and P. Ding, "Study on mechanical behavior of prefabricated assembled metro station structure after assembly," *Modern Tunneling Technology*, vol. 55, pp. 115–123, 2018.
[26] Z. Duan, *Mechanical Test and Construction Process Simulation of Epoxy Toughening Materials of Mortise and Tenon Joints in Assembled Metro Station*, Shandong University, 2021.
[27] X. Y. Chen, "Experimental study on mechanical properties of assembled underground station structures," *Reviews on Advanced Materials Science*, vol. 6, no. 1, pp. 578–590, 2019.
[28] X. Yang, F. Lin, and M. Huang, "Analysis of the law of joint deformation for grouted mortise–tenon joint," *Advances in Civil Engineering*, vol. 2022, Article ID 2909993, 13 pages, 2022.
[29] X. R. Yang, "Theory and practice of prefabricated assembled structures for mined metro stations," *Tunnelling and Underground Space Technology*, vol. 108, Article ID 103717, 2020.